

Phase-dependent fluctuations of intermittent resonance fluorescence

Héctor M. Castro-Beltrán,^{1,2,*} Ricardo Román-Ancheyta,^{2,†} and Luis Gutiérrez^{1,‡}

¹*Centro de Investigación en Ingeniería y Ciencias Aplicadas,
Instituto de Investigación en Ciencias Básicas y Aplicadas,
Universidad Autónoma del Estado de Morelos, Avenida Universidad 1001, 62209 Cuernavaca, Morelos, México*

²*Instituto de Ciencias Físicas, Universidad Nacional Autónoma de México,
Apartado Postal 48-3, 62251 Cuernavaca, Morelos, México*

(Dated: July 28, 2021)

Electron shelving gives rise to bright and dark periods in the resonance fluorescence of a three-level atom. The spectral signature of such blinking is a very narrow inelastic peak on top of the two-level atom spectrum. Here, we investigate theoretically phase-dependent fluctuations (e.g., squeezing) of intermittent resonance fluorescence in the frameworks of balanced and conditional homodyne detection (BHD and CHD, respectively). In BHD, the squeezing is reduced significantly in size and Rabi frequency range compared to that for a two-level atom. The sharp peak is found only in the spectrum of the squeezed quadrature, splitting the negative broader squeezing peak for weak fields. CHD correlates the BHD signal with the detection of emitted photons. It is thus sensitive to third-order fluctuations of the field, produced by the atom-laser nonlinearity, that cause noticeable deviations from the second-order BHD results. For weak driving, the third-order spectrum is negative, enlarging the squeezing peak but also reducing the sharp peak. For strong driving, the spectrum is dominated by third-order fluctuations, with a large sharp peak and the sidebands becoming dispersive. Finally, the addition of third-order fluctuations makes the integrated spectra of both quadratures equal in magnitude in CHD, in contrast to those by BHD. A simple mathematical approach allows us to obtain very accurate analytical results in the shelving regime.

PACS numbers: 42.50.Lc, 42.50.Ct, 42.50.Hz

I. INTRODUCTION

A photon emitter with peculiar fluctuations is a single three-level atom with a laser-driven strong transition competing with a coherently or incoherently driven weak transition. The occasional population of a long-lived state, an effect called electron shelving, produces intermittence (blinking) in the resonance fluorescence of the strong transition. Photon statistics of the fluorescence have been thoroughly studied for three-level atomic systems [1], in which case the process is ergodic, i.e., when the mean bright and dark periods are finite. For a single quantum dot or molecule the statistics are more complicated if the process is not ergodic [2]. In the spectral domain, ergodic shelving manifests in the appearance of a very narrow inelastic peak on top of the central peak of the two-level-like spectrum. This has been well studied analytically and numerically [3–5] and observed experimentally [6]. In the latter, heterodyne detection was used, which allows for very high spectral resolution [7]. In their paper [6], Bühner and Tamm suggest performing complementary phase-dependent measurements of the fluorescence; so far, there are no reports yet, perhaps due to experimental restrictions.

Squeezing, the reduction of fluctuations below those of a coherent state in a quadrature at the expense of in-

creasing fluctuations in the other quadrature, is weak in resonance fluorescence [8, 9]. The low collection and imperfect quantum efficiency of photodetectors have been the main barriers for the observation of squeezing, although recent experimental progress tackle these issues. On the one hand, there is the increased solid angle of emission captured with minimal disturbance of the photon density of states surrounding the atom [10]. On the other hand, there is the development of conditional detection schemes based on homodyne detection that cancel the finite quantum efficiency issue [11–18]. We discuss two of them.

Homodyne correlation measurement (HCM), proposed by Vogel [11, 12] (see also [19]), consists of intensity correlations of the previously mixed source and weak local oscillator fields, thus canceling the detector efficiency factors. The output contains several terms, including the variance and an amplitude-intensity correlation. Very recently, HCM was used to observe squeezing in the resonance fluorescence of a single two-level quantum dot [20] in conditions close to those for free-space atomic resonance fluorescence. In fact, in the first demonstration of HCM the amplitude-intensity correlation of the fluorescence of a single three-level ion in the Λ configuration was observed [21] although not yet in the squeezing regime.

Conditional homodyne detection (CHD) was proposed and demonstrated by Carmichael, Orozco and coworkers [13, 14]. This consists of balanced homodyne detection (BHD) of a quadrature conditioned on an intensity measurement of part of the emitted field; it gives the amplitude-intensity correlation of HCM but measured directly, without the other terms. As in the inten-

*Electronic address: hcastro@uaem.mx

†Electronic address: ancheyta6@gmail.com

‡Electronic address: luis.gutierrez@uaem.mx

sity correlations, the conditioning cancels the dependence on detector efficiency. The intensity detection channel has nontrivial effects on the quadrature signals. The amplitude-intensity correlation is of third order in the field amplitude; hence it allows for third-order fluctuations. Initially, CHD was devised for weak light emitters, neglecting the third-order fluctuations. This allowed the identification of the Fourier transform of the correlation as the spectrum of squeezing [13, 14]. However, recent work on CHD of two-level atom resonance fluorescence has shown important deviations from the spectrum of squeezing due to increasing nonlinearity in the atom-laser interaction [22, 23]. An additional display of these non-Gaussian fluctuations is found in the asymmetry of the correlation in cavity QED [24] and in the resonance fluorescence of a V-type three-level atom [25–27] and of two blockading Rydberg atoms [28].

In this paper we investigate theoretically ensemble-averaged phase-dependent fluctuations of the intermittent (ergodic) resonance fluorescence of a single three-level atom (3LA). Besides numerical solutions for the one- and two-time expectation values, we obtain approximate analytical solutions which are very accurate in the limit when the decay rate of the strong transition is much larger than those of the weak transitions. Our solutions are simple and reflect clearly the time and spectral scales. Thus we begin by writing the expression for the coherent and phase-independent incoherent spectra of the 3LA, studied numerically at length in Ref. [5].

We compare the spectra and variances of an ideal BHD approach, which could also be obtained from HCM, with those of the CHD method. They have in common that the sharp extra peak [3–6], on atom-laser resonance, is a feature *only* of the quadrature that features squeezing; in the other quadrature the spectrum is a simple broad positive Lorentzian. In the weak-field limit, while both methods give similar negative spectra for a two-level atom (2LA), the sharp peak is positive, reducing the squeezing in BHD and enhancing the negative peak in CHD. For a strong laser field the third-order fluctuations of CHD distort the positive Lorentzian sidebands of the Mollow triplet and turn them dispersive for both 2LA and 3LA. However, for the 3LA, both the sharp peak and the dispersive sidebands are much larger than the second-order spectrum.

Interestingly, in CHD, the addition of third-order fluctuation makes the integrated spectra of both quadratures equal in magnitude, in contrast to the case of the spectrum by BHD [23]. This feature of CHD may be a bonus over other modern variations of the standard homodyne detection scheme.

This paper is organized as follows: In Sec. II we introduce the atom-laser model and obtain approximate analytic solutions in the shelving regime. In Sec. III we calculate the phase-independent spectrum, and in Sec. IV we calculate the phase-dependent spectra and variances. Sections V and VI are devoted to the amplitude-intensity correlation by CHD and its spectrum, respec-

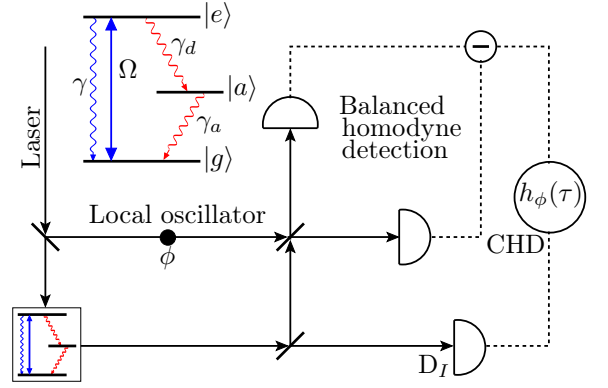


FIG. 1: (Color online) Scheme of conditional homodyne detection. Blocking the path to the lower detector, D_I , realizes the standard balanced homodyne detection. The inset shows the three-level atom-laser interaction and spontaneous decays.

tively. Finally, conclusions are given in Sec. VII. Two appendices summarize the analytic and numerical methods employed.

II. ATOM-LASER MODEL AND SOLUTIONS

We consider a single three-level atom where a laser of Rabi frequency Ω drives a transition between the ground state $|g\rangle$ and an excited state $|e\rangle$. The excited state has two spontaneous emission channels: one directly to the ground state with rate γ for the driven transition, and one via a long-lived shelving state $|a\rangle$ with rate γ_d , which in turn decays to the ground state with rate γ_a (see Fig. 1). In the limit

$$\gamma \gg \gamma_d, \gamma_a \quad (1)$$

the fluorescence of the driven transition features well-defined bright and dark periods of average lengths,

$$T_B = \frac{2\Omega^2 + \gamma^2}{\gamma_d\Omega^2}, \quad T_D = \gamma_a^{-1}, \quad (2)$$

respectively, as calculated in Ref. [5] using a random telegraph model.

Throughout this paper we assume zero atom-laser detuning. This serves two purposes: first, we limit the discussion to the essentials of the main topics; second, with further assumptions discussed later, we obtain close approximate analytical solutions. The master equation for the atomic density operator, in the frame rotating at the laser frequency, can be written as

$$\begin{aligned} \dot{\rho}(t) = & -i\frac{\Omega}{2}[\sigma_{eg} + \sigma_{ge}, \rho] \\ & + \frac{\gamma}{2}(2\sigma_{ge}\rho\sigma_{eg} - \sigma_{ee}\rho - \rho\sigma_{ee}) \\ & + \frac{\gamma_d}{2}(2\sigma_{ae}\rho\sigma_{ea} - \sigma_{ee}\rho - \rho\sigma_{ee}) \\ & + \frac{\gamma_a}{2}(2\sigma_{ga}\rho\sigma_{ag} - \sigma_{aa}\rho - \rho\sigma_{aa}), \end{aligned} \quad (3)$$

where $\sigma_{jk} = |j\rangle\langle k|$ are atomic transition operators which obey the inner product prescription $\langle j|k\rangle = \delta_{jk}$.

We obtain two sets of equations. The first one is

$$\dot{\rho} = \mathbf{M}\rho + \mathbf{b}, \quad (4a)$$

where $\rho = (\rho_{eg}, \rho_{ge}, \rho_{ee}, \rho_{gg})^T$, $\mathbf{b} = (0, 0, 0, \gamma_a)^T$, and

$$\mathbf{M} = \begin{pmatrix} -\gamma_+/2 & 0 & i\Omega/2 & -i\Omega/2 \\ 0 & -\gamma_+/2 & -i\Omega/2 & i\Omega/2 \\ i\Omega/2 & -i\Omega/2 & -\gamma_+ & 0 \\ -i\Omega/2 & i\Omega/2 & \gamma_- & -\gamma_a \end{pmatrix}, \quad (4b)$$

where

$$\gamma_+ = \gamma + \gamma_d, \quad \gamma_- = \gamma - \gamma_a. \quad (5)$$

Here, we have eliminated the population ρ_{aa} due to conservation of probability, $\rho_{gg} + \rho_{ee} + \rho_{aa} = 1$.

The second set of equations involves the coherences linking states $|e\rangle$ and $|g\rangle$ to state $|a\rangle$, i.e., $(\rho_{ga}, \rho_{ag}, \rho_{ea}, \rho_{ae})^T$. They evolve with damped oscillations with zero mean. The two sets are decoupled, and only the first one is relevant for the purposes of this work.

We obtain first the steady state of the density operator (labeled with the abbreviation *st*). For a more compact notation we define $\alpha_- = \rho_{eg}^{st} = \langle \sigma_- \rangle_{st}$, $\alpha_+ = \alpha_-^*$, and $\alpha_{jj} = \rho_{jj}^{st} = \langle \sigma_{jj} \rangle_{st}$. We have

$$\alpha_{\mp} = \mp i \frac{Y/\sqrt{2}}{1 + Y^2 + (q/2)Y^2}, \quad (6a)$$

$$\alpha_{ee} = \frac{Y^2/2}{1 + Y^2 + (q/2)Y^2}, \quad (6b)$$

$$\alpha_{gg} = \frac{1 + Y^2/2}{1 + Y^2 + (q/2)Y^2}, \quad (6c)$$

$$\alpha_{aa} = q\alpha_{ee}, \quad (6d)$$

where

$$q = \gamma_d/\gamma_a, \quad Y = \sqrt{2}\Omega/\gamma_+. \quad (7)$$

For $\gamma_d = 0$ ($q = 0$) we recover the results of the 2LA.

Equation (4a) is still too complicated to solve analytically in the general case. However, in the limit (1), very good approximate solutions are obtained (see Appendix A for more details). We use a Laplace transform approach to obtain approximate expectation values of the atomic vector, $\mathbf{s} = (\sigma_-, \sigma_+, \sigma_{ee}, \sigma_{gg})^T$, and two-time correlations. With the atom initially in its ground state, $\langle \mathbf{s}(0) \rangle = (0, 0, 0, 1)^T$, the expectation values of the atomic operators are

$$\begin{aligned} \langle \sigma_{\mp}(t) \rangle &= \mp i \frac{Y/\sqrt{2}}{1 + Y^2} f(t) \mp i \frac{\sqrt{2}\gamma_+ Y}{8\delta} (e^{\lambda_+ t} - e^{\lambda_- t}) \\ &\quad + \alpha_{\mp} (1 - e^{\lambda_2 t}), \end{aligned} \quad (8a)$$

$$\langle \sigma_{ee}(t) \rangle = \frac{Y^2/2}{1 + Y^2} f(t) + \alpha_{ee} (1 - e^{\lambda_2 t}), \quad (8b)$$

$$\langle \sigma_{gg}(t) \rangle = e^{\lambda_2 t} - \frac{Y^2/2}{1 + Y^2} f(t) + \alpha_{gg} (1 - e^{\lambda_2 t}), \quad (8c)$$

where

$$\begin{aligned} f(t) &= e^{\lambda_2 t} - \frac{1}{2} \left[\left(1 + \frac{3\gamma_+}{4\delta} \right) e^{\lambda_+ t} \right. \\ &\quad \left. + \left(1 - \frac{3\gamma_+}{4\delta} \right) e^{\lambda_- t} \right], \end{aligned} \quad (9)$$

$$\lambda_1 = -\gamma_+/2, \quad (10a)$$

$$\lambda_2 = -\gamma_a \left(1 + q \frac{\Omega^2}{2\Omega^2 + \gamma^2} \right), \quad (10b)$$

$$\lambda_{\pm} = -\frac{3\gamma_+}{4} \pm \delta, \quad (10c)$$

and

$$\delta = (\gamma_+/4) \sqrt{1 - 8Y^2}. \quad (11)$$

This approach allows us to identify Eqs. (10) as the eigenvalues of the matrix (4b) of the master equation. This is much more convenient than attempting to write the exact ones in compact form. The eigenvalues contain the kernel of the atomic evolution, that is, the scales of decay and coherent evolution, as well as the corresponding widths and positions of the spectral components.

The first eigenvalue, λ_1 , is exact and gives half the total decay rate from the excited state. Although absent in Eqs. (8), it occurs in the second-order correlations (see below). Then, λ_2 represents the slow decay rate due to shelving. This causes the steady state to be reached after a long time, $t \sim \gamma_d^{-1}$. Borrowing from the random telegraph model [5], the slow decay rate is given by $\lambda_2 = -(T_D^{-1} + T_B^{-1})$. The two remaining eigenvalues represent the damped coherent evolution; they are real if $8Y^2 \leq 1$ and complex if $8Y^2 > 1$. Eigenvalues λ_1, λ_{\pm} contain the two-level-like evolution towards a quasi-steady state (with the decay rate γ of the two-level case replaced by γ_+ for the 3LA) that is followed by the slow decay.

The two-time correlations $\langle \sigma_+(0) \mathbf{s}(\tau) \sigma_-(0) \rangle_{st}$, which have initial conditions $(0, 0, 0, \alpha_{ee})^T$, are approached like those for $\langle \mathbf{s}(t) \rangle$. Using the quantum regression formula (see, e.g., [29]) and $\mathbf{s}(0) = (0, 0, 0, 1)^T$, we have

$$\langle \sigma_+(0) \mathbf{s}(\tau) \sigma_-(0) \rangle_{st} = \alpha_{ee} \langle \mathbf{s}(\tau) \rangle_{\mathbf{s}(0)}, \quad (12)$$

that is, these correlations are identical to Eqs. (8) times the factor α_{ee} , with t replaced by τ .

The approximate analytic solutions to the correlations $\langle \sigma_+(0) \mathbf{s}(\tau) \rangle_{st}$, which have initial conditions $(\alpha_{ee}, 0, 0, \alpha_+)^T$, can be similarly obtained (see Appendix A). We use them, however, to obtain the solutions for correlations of fluctuations, $\langle \Delta \sigma_+(0) \Delta \mathbf{s}(\tau) \rangle_{st}$, where

$$\Delta \sigma_{jk}(t) = \sigma_{jk}(t) - \langle \sigma_{jk} \rangle_{st}, \quad \langle \Delta \sigma_{jk}(t) \rangle = 0. \quad (13)$$

Hence

$$\langle \Delta \sigma_+(0) \Delta \sigma_{\mp}(\tau) \rangle_{st} = \langle \sigma_+(0) \sigma_{\mp}(\tau) \rangle_{st} - \langle \sigma_+ \rangle_{st} \langle \sigma_{\mp} \rangle_{st}, \quad (14)$$

yielding

$$\langle \Delta\sigma_+(0)\Delta\sigma_-(\tau) \rangle_{st} = C_1 e^{\lambda_1 \tau} \pm C_2 e^{\lambda_2 \tau} \mp C_+ e^{\lambda_+ \tau} \mp C_- e^{\lambda_- \tau}, \quad (15)$$

where

$$C_1 = \frac{Y^2/4}{1 + Y^2 + (q/2)Y^2}, \quad (16a)$$

$$C_2 = \frac{qY^4/4}{(1 + Y^2)(1 + Y^2 + (q/2)Y^2)^2}, \quad (16b)$$

$$C_{\mp} = \frac{Y^2[1 - Y^2 \pm (1 - 5Y^2)(\gamma_+/4\delta)]}{8(1 + Y^2)(1 + Y^2 + (q/2)Y^2)}. \quad (16c)$$

III. STATIONARY POWER SPECTRUM

The stationary (Wiener-Khintchine) power spectrum is given by the Fourier transform of the dipole field autocorrelation function,

$$S(\omega) = \frac{1}{\pi\alpha_{ee}} \text{Re} \int_0^\infty d\tau e^{-i\omega\tau} \langle \sigma_+(0)\sigma_-(\tau) \rangle_{st}. \quad (17)$$

The factor $(\pi\alpha_{ee})^{-1}$ normalizes the integral of $S(\omega)$ over all frequencies to unity. Equation (14) separates the spectrum in two parts:

$$S(\omega) = S_{coh}(\omega) + S_{inc}(\omega), \quad (18)$$

where

$$S_{coh}(\omega) = \frac{|\alpha_+|^2}{\pi\alpha_{ee}} \text{Re} \int_0^\infty e^{-i\omega\tau} d\tau = \frac{|\alpha_+|^2}{\pi\alpha_{ee}} \delta(\omega) \quad (19)$$

and

$$S_{inc}(\omega) = \frac{1}{\pi\alpha_{ee}} \text{Re} \int_0^\infty d\tau e^{-i\omega\tau} \langle \Delta\sigma_+(0)\Delta\sigma_-(\tau) \rangle_{st} \quad (20)$$

are, respectively, the coherent spectrum, due to elastic scattering, and the incoherent (inelastic) spectrum, due to atomic fluctuations.

The main features of the spectrum of the atom-laser system of the previous section were studied in [5]. The incoherent spectrum consists of a two-level-like structure that becomes a triplet for strong excitation [30], plus a sharp peak, associated with the eigenvalue λ_2 , due to the shelving of the electronic population in the long-lived state. This three-level system contains the essential physics of the more complex atomic system used for the experimental observation of the sharp peak [6] by heterodyne detection, able to resolve hertz or sub-hertz features [7]. The sharp peak had been predicted for the V-type and Λ -type 3LAs [3, 4], which also feature electron shelving.

Our Laplace transform approach allowed us to obtain a very good analytic approximation to the full spectrum,

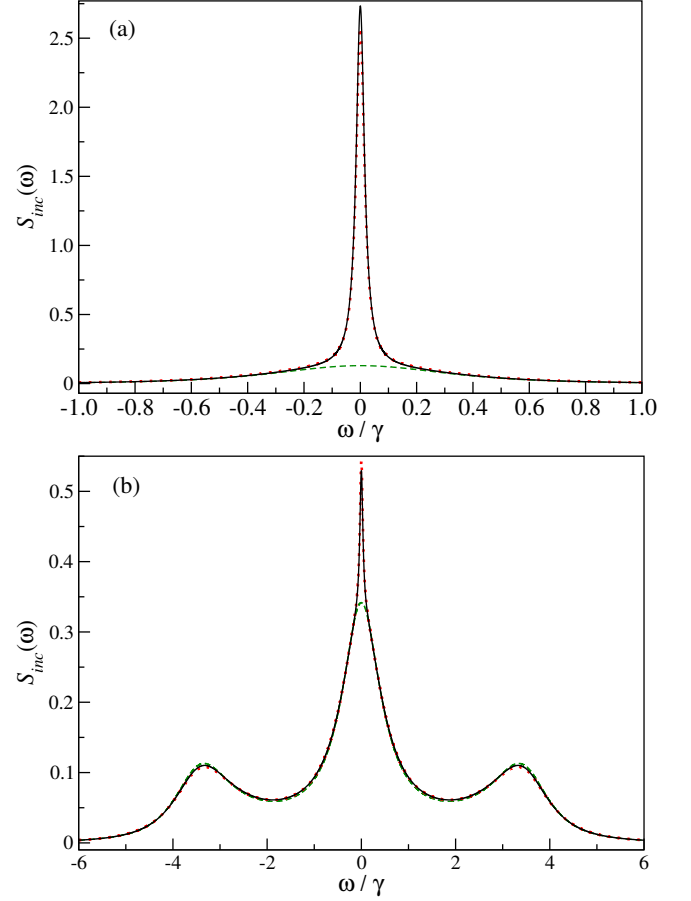


FIG. 2: (Color online) Incoherent spectrum for (a) a saturating laser field, $\Omega = \gamma_+/4 = 0.2625\gamma$, and (b) a strong field, $\Omega = 3.5\gamma$, with $\gamma_d = 0.05\gamma$ and $\gamma_a = 0.015\gamma$. The solid black and dotted red curves are, respectively, the exact and approximate spectra, and the dashed green curve is the 2LA spectrum.

split into its various components, with their widths and amplitudes readily spotted. Substituting Eq. (15) into Eq. (20) the incoherent spectrum is

$$S_{inc}(\omega) = \frac{1}{\pi\alpha_{ee}} \left[C_+ \frac{\lambda_+}{\omega^2 + \lambda_+^2} + C_- \frac{\lambda_-}{\omega^2 + \lambda_-^2} - C_1 \frac{\lambda_1}{\omega^2 + \lambda_1^2} - C_2 \frac{\lambda_2}{\omega^2 + \lambda_2^2} \right]. \quad (21)$$

In Fig. 2 we plot this spectrum with eigenvalues (10) along the exact and 2LA spectra. It reproduces remarkably well the exact spectrum, with the sharp peak being slightly smaller (bigger) in the saturating (strong) case than the exact one. Also, making $\gamma_d = 0$, the formula is exact for the 2LA spectrum [30]. The intensity (integral over all frequencies) of the sharp peak is

$$I_{ep} = \frac{qY^2/2}{(1 + Y^2)(1 + Y^2 + (q/2)Y^2)}.$$

It is small for both weak and strong driving (proportional to Y^2 and Y^{-2} , respectively), and largest for $\Omega \approx 3\gamma/4$.

The coherent spectrum of the 3LA is

$$S_{coh}(\omega) = \frac{1}{\pi(1 + Y^2 + (q/2)Y^2)}\delta(\omega), \quad (22)$$

smaller than that of the 2LA (where $q = 0$) [5]. The difference in intensity is precisely given by I_{ep} .

The choice of values $\gamma_d = 0.05\gamma$ and $\gamma_a = 0.015\gamma$, small enough to fulfill the limit (1), is such that the relation $\gamma_d = 3.3\gamma_a$ closely optimizes the intensity of the sharp extra peak for any given Rabi frequency [5]. For simplicity, we use these values for all the remaining 3LA plots in this work.

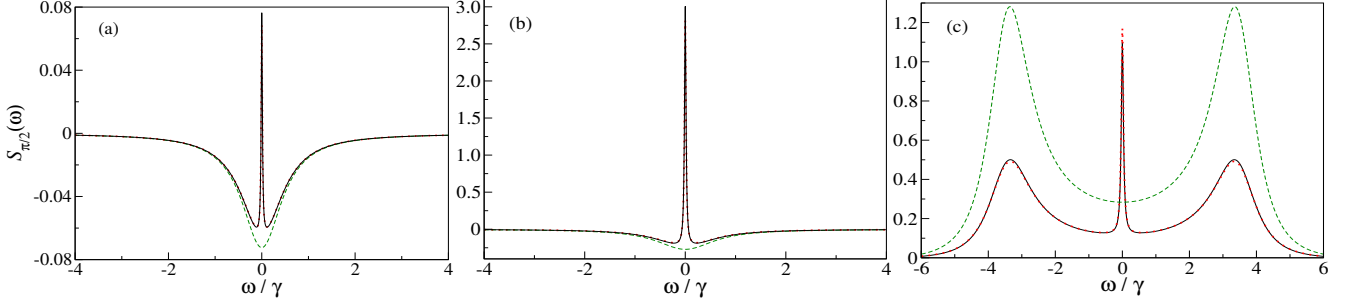


FIG. 3: (Color online) Spectra of the $\phi = \pi/2$ quadrature for (a) $\Omega = 0.1\gamma$, (b) $\Omega = 0.2625\gamma$, and (c) $\Omega = 3.5\gamma$. The other parameters are $\gamma_d = 0.05\gamma$, $\gamma_a = 0.015\gamma$, and $\eta = 1$. The solid black and dotted red lines correspond to the exact and approximate 3LA spectra, respectively, and the dashed green lines are the 2LA spectra.

IV. THE SPECTRUM OF SQUEEZING

Now we turn to the phase-dependent spectrum of the fluorescence of the three-level atom and compare it to the well-known case of the two-level atom [9, 31]. Following Carmichael [32], we define the *ideal source field* spectrum of squeezing as the Fourier transform of photocurrent fluctuations of the quadratures in homodyne detection,

$$\begin{aligned} S_\phi(\omega) &= 8\gamma_+\eta \int_0^\infty d\tau \cos \omega\tau \langle : \Delta\sigma_\phi(0)\Delta\sigma_\phi(\tau) : \rangle_{st} \\ &= 8\gamma_+\eta \int_0^\infty d\tau \cos \omega\tau \\ &\quad \times \text{Re} [e^{-i\phi} \langle \Delta\sigma_+(0)\Delta\sigma_\phi(\tau) \rangle_{st}], \end{aligned} \quad (23)$$

where

$$\Delta\sigma_\phi = \frac{1}{2} (\Delta\sigma_- e^{i\phi} + \Delta\sigma_+ e^{-i\phi}), \quad (24)$$

ϕ is the phase of the local oscillator in a BHD setup (that is, blocking the path to detector D_I in Fig. 1), η is a combined collection and detection efficiency, and the dots $::$ indicate that the operators must follow time and normal orderings. This is an incoherent spectrum as it depends on the field fluctuations. In fact, the phase-dependent and the phase-independent spectra are related as [31]

$$S_{inc}(\omega) = \frac{1}{8\pi\alpha_{ee}\gamma_+\eta} [S_\phi(\omega) + S_{\phi+\pi/2}(\omega)]. \quad (25)$$

Adding the spectra for $\phi = 0$ and $\pi/2$ Eq. (20) is recovered.

Although the atom and laser parameters do not always allow for squeezing (negative values in the spectrum), we keep the moniker of spectrum of squeezing in order to distinguish this from the spectrum of Sec. VI.

Substituting Eq. (15) in Eq. (23) the approximate spectra for the quadratures are

$$S_0(\omega) = -8\gamma_+\eta C_1 \frac{\lambda_1}{\omega^2 + \lambda_1^2}, \quad (26)$$

$$\begin{aligned} S_{\pi/2}(\omega) &= 8\gamma_+\eta \left[C_+ \frac{\lambda_+}{\omega^2 + \lambda_+^2} + C_- \frac{\lambda_-}{\omega^2 + \lambda_-^2} \right. \\ &\quad \left. - C_2 \frac{\lambda_2}{\omega^2 + \lambda_2^2} \right]. \end{aligned} \quad (27)$$

For $\phi = 0$ the spectrum is only a single, positive (no squeezing) Lorentzian, just like for the 2LA, now with a width of $\gamma_+/2$. For $\phi = \pi/2$ the spectrum is more interesting, as shown in Fig. 3 for several field strengths. For instance, it has a sharp peak [last term in Eq. (27)], with its maximum near $\Omega \approx 0.9\gamma$. From weak to little more than saturating fields the first two terms of Eq. (27) (with factors $C_\pm|\lambda_\pm|$) add to form a single negative peak, indicating squeezing. Rice and Carmichael [31] found that the weak-field spectrum ($Y^2 \ll 1$) in the 2LA has a line-width smaller than $\gamma/2$ due to the negative value of the Lorentzians with amplitudes $C_\pm|\lambda_\pm|$ in Eq. (21), resulting in a squared Lorentzian [30]. In

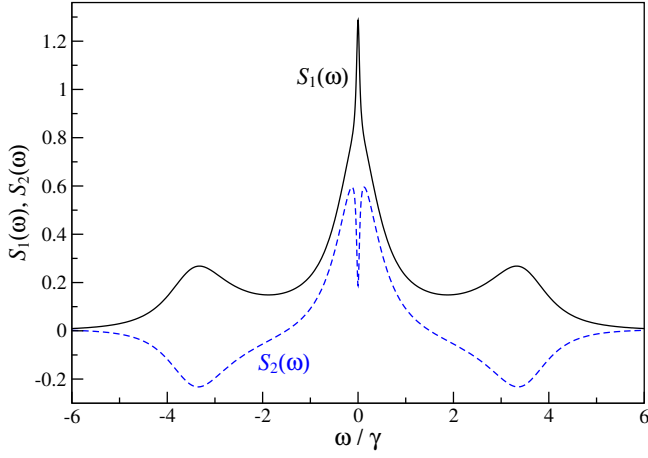


FIG. 4: (Color online) Spectra of the noise correlations $\langle \Delta\sigma_+(0)\Delta\sigma_+(\tau) \rangle_{st}$ ($S_1(\omega)$, solid line) and $\langle \Delta\sigma_+(0)\Delta\sigma_-(\tau) \rangle_{st}$ ($S_2(\omega)$, dashed line) for $\Omega = 3.5\gamma$, $\gamma_d = 0.05\gamma$, $\gamma_a = 0.015\gamma$, and $\eta = 1$.

the 3LA there is less squeezing and the sharp peak splits the squeezing peak. For strong fields, the spectrum consists of the sidebands of the Mollow triplet plus the extra peak.

An additional manifestation of shelving is the shrinking of the sidebands of the quadrature spectra compared to those of the 2LA. This is because state $|a\rangle$ takes up an important fraction of the steady-state population (actually, $\alpha_{aa} = q\alpha_{ee}$) for increasing Rabi frequency.

To further illustrate the difference among the spectra of quadratures, we plot in Fig. 4 the spectra of the correlations $\langle \Delta\sigma_+(0)\Delta\sigma_{\mp}(\tau) \rangle_{st}$. For $S_0(\omega)$ the integrals are added, while for $S_{\pi/2}(\omega)$ they are subtracted. Thus, the sharp peak appears only in the latter. The addition or subtraction cancels spectral components. The spectrum (20) contains only one of the integrals.

A. Variances and integrated spectra

An alternative approach to squeezing is the study of the variance or noise in a quadrature,

$$V_\phi = \langle :(\Delta\sigma_\phi)^2: \rangle_{st} = \text{Re} [e^{-i\phi} \langle \Delta\sigma_+ \Delta\sigma_\phi \rangle_{st}] \quad (28)$$

or, equivalently, the integrated spectrum, related as $\int_{-\infty}^{\infty} S_\phi(\omega) d\omega = 4\pi\gamma_\eta V_\phi$. A negative variance is a signature of squeezing in a quadrature. We have

$$V_0 = 2C_1 = \frac{Y^2/2}{1 + Y^2 + (q/2)Y^2}, \quad (29a)$$

$$\begin{aligned} V_{\pi/2} &= 2(C_2 - C_+ - C_-) \\ &= \frac{Y^2/2}{(1 + Y^2)(1 + Y^2 + (q/2)Y^2)^2} \\ &\quad \times \left[Y^4 \left(1 + \frac{q}{2} \right) + \frac{q}{2} Y^2 - 1 \right]. \end{aligned} \quad (29b)$$

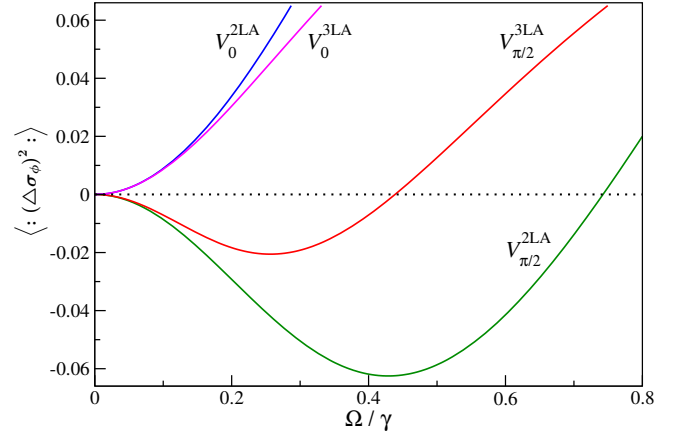


FIG. 5: (Color online) Variance of two and three-level atom resonance fluorescence for weak to moderately strong excitation, using Eqs. (29). Additional parameters for the 3LA are $\gamma_d = 0.05\gamma$, $\gamma_a = 0.015\gamma$, and $\eta = 1$.

We plot the variances in Fig. 5. V_0 is positive for any laser strength; there is no squeezing for $\phi = 0$ but the total noise is smaller for the 3LA. For $V_{\pi/2}$ both the interval of the laser strength and amplitude for squeezing are notably reduced by the coupling to the long-lived state, and the Rabi frequency for the largest negative value is now very close to the saturating value, $\Omega = \gamma_+/4$, which we use for several spectra.

The standard BHD technique depends on the finite detector efficiency η . This is a key obstacle to observe the weak squeezing of single-atom resonance fluorescence. Only very recently has the squeezing in the fluorescence of a single two-level quantum dot been observed [20] with homodyne correlation measurements [11, 12], which are independent of the detector efficiency. However, the measured variance had to be extracted from complementary measurements with different phases.

There is a subtle issue that also has to be addressed: Why is it that the quadrature variances are different? It seems natural to think that one features squeezing and the other does not. But, from the viewpoint of integrated spectra, one could expect this to be independent of the local oscillator phase. Thus, we reformulate the question: What spectrum could be integrated that gives the same value for both quadratures?

Conditional homodyne detection also solves the issue of finite detector efficiency, measuring an amplitude-intensity correlation, in this case without the need to extract the desired correlation from complementary measurements. CHD has been used to detect squeezing of a cavity QED source [14]. Additionally, CHD gives an answer to the missing term in the integrated spectra. We devote the next two sections to a summary of CHD theory and its application to 3LA resonance fluorescence.

V. CONDITIONAL HOMODYNE DETECTION

Figure 1 illustrates the setup for amplitude-intensity correlation by CHD. Its theory was first presented in [13]; its application to resonance fluorescence of a 2LA was given in [22, 23], and its application to that of a V-type three-level atom was presented in [25–27]. Hence, here we show only its basic features. A quadrature of the field, E_ϕ , is measured in balanced homodyne detection conditioned on the direct detection of a photon (intensity, I) at detector D_I , i.e., $\langle I(0)E_\phi(\tau) \rangle_{st}$. Here, $E_\phi \propto \sqrt{\eta}\sigma_\phi$ and $I \propto \eta\sigma_+\sigma_-$. Upon normalization, the dependence of the correlation on the detector efficiency η is canceled. Then

$$h_\phi(\tau) = \frac{\langle : \sigma_+(0)\sigma_-(0)\sigma_\phi(\tau) : \rangle_{st}}{\langle \sigma_+\sigma_- \rangle_{st} \langle \sigma_\phi \rangle_{st}}, \quad (30)$$

where it is assumed that the system is stationary,

$$\sigma_\phi = \frac{1}{2} (\sigma_- e^{i\phi} + \sigma_+ e^{-i\phi}) \quad (31)$$

is the dipole quadrature operator, ϕ is the phase between the strong local oscillator and the driving field, and we recall that $::$ indicates time and normal operator orderings. These orderings lead to different formulas for positive and negative time intervals, and in general, the correlations are asymmetric [13, 14, 24–28]. However, in the present case the correlation is symmetric; thus we only use the expression for positive intervals:

$$h_\phi(\tau) = \frac{\langle \sigma_+(0)\sigma_\phi(\tau)\sigma_-(0) \rangle_{st}}{\langle \sigma_+\sigma_- \rangle_{st} \langle \sigma_\phi \rangle_{st}}. \quad (32)$$

When the laser excites the atom on resonance, as is the case in this paper, the in-phase quadrature $\langle \sigma_{\phi=0}(t) \rangle$ vanishes at all times, and likewise $\langle \sigma_+(0)\sigma_0(\tau)\sigma_-(0) \rangle_{st} = 0$. So, to obtain a finite measurement of this quadrature, it is necessary to add a coherent offset of amplitude E_{off} and phase $\phi = 0$ to the dipole field before reaching the beam splitter [22]. This procedure, however, hides the non-classical character of the fluorescence, showing a monotonously decaying correlation:

$$h_0(\tau) = 1 + \frac{\alpha_{ee}}{\alpha_{ee} + E_{\text{off}}^2} e^{-\gamma_+ \tau/2}. \quad (33)$$

The $\phi = \pi/2$ quadrature is more interesting. Substituting Eqs. (8a), (12) and (6b) into Eq. (32) we obtain

$$h_{\pi/2}(\tau) = 1 + B_2 e^{\lambda_2 \tau} - B_+ e^{\lambda_+ \tau} - B_- e^{\lambda_- \tau}, \quad (34)$$

where

$$B_2 = q \frac{Y^2/2}{1 + Y^2}, \quad (35a)$$

$$B_\pm = \left(1 + q \frac{Y^2/2}{1 + Y^2} \right) \left(\frac{1}{2} \pm \frac{1 - 2Y^2}{8\delta/\gamma_+} \right). \quad (35b)$$

The coupling to the metastable level $|a\rangle$ has visible consequences for both short and long times, making the CHD

correlation amplitude larger than is the case for a 2LA, through the factor $q = \gamma_d/\gamma_a$. This excess amplitude decays slowly towards the unit value, which signals the decorrelation for long τ , best noticed for large Ω .

The CHD correlation can be written in terms of correlations of fluctuation operators, as is the case with the full incoherent and squeezing spectra. Splitting the dipole operators into a mean plus fluctuations, Eq. (13), $h_\phi(\tau)$ is decomposed into a constant term plus two two-time correlations, one of second order and one of third order in the dipole fluctuation operators,

$$h_\phi(\tau) = 1 + h_\phi^{(2)}(\tau) + h_\phi^{(3)}(\tau), \quad (36a)$$

where

$$h_\phi^{(2)}(\tau) = \frac{2\text{Re}[\langle \sigma_- \rangle_{st} \langle \Delta\sigma_+(0)\Delta\sigma_\phi(\tau) \rangle_{st}]}{\langle \sigma_\phi \rangle_{st} \langle \sigma_+\sigma_- \rangle_{st}}, \quad (36b)$$

$$h_\phi^{(3)}(\tau) = \frac{\langle \Delta\sigma_+(0)\Delta\sigma_\phi(\tau)\Delta\sigma_-(0) \rangle_{st}}{\langle \sigma_\phi \rangle_{st} \langle \sigma_+\sigma_- \rangle_{st}}. \quad (36c)$$

The splitting is not done by the measurement scheme, but it can be calculated to provide valuable information about the system's fluctuations.

For $\phi = 0$, due to the need to add an offset, we are left with Eq. (33). For $\phi = \pi/2$ we obtain the approximate expression:

$$h_{\pi/2}^{(2)}(\tau) = \frac{2}{\alpha_{ee}} [C_2 e^{\lambda_2 \tau} - C_+ e^{\lambda_+ \tau} - C_- e^{\lambda_- \tau}] \quad (37a)$$

$$h_{\pi/2}^{(3)}(\tau) = D_2 e^{\lambda_2 \tau} + D_+ e^{\lambda_+ \tau} + D_- e^{\lambda_- \tau}, \quad (37b)$$

where

$$D_2 = B_2 - \frac{2C_2}{\alpha_{ee}}, \quad D_\pm = \frac{2C_\pm}{\alpha_{ee}} - B_\pm, \quad (37c)$$

which are too cumbersome to be reproduced in full here. In Fig. 6 we plot the analytical results, Eq. (34) and its partial results $1 + h_{\pi/2}^{(2)}(\tau)$ and $h_{\pi/2}^{(3)}(\tau)$, which differ very little from the exact ones.

The vanishing of Eq. (36a) at $\tau = 0$ has the same origin as the antibunching in the intensity correlations: when the atom is in the ground state upon a photon emission, both the dipole field and the intensity are zero, and they build up again when the atom reabsorbs light. For $\phi = 0$ the effect is not seen due to the additional offset. So

$$\begin{aligned} h_{\pi/2}^{(2)}(0) &= \frac{\alpha_{ee} - 2|\alpha_+|^2}{\alpha_{ee}} \\ &= \frac{Y^2 + (q/2)Y^2 - 1}{1 + Y^2 + (q/2)Y^2}, \end{aligned} \quad (38a)$$

and

$$\begin{aligned} h_{\pi/2}^{(3)}(0) &= \frac{2(|\alpha_+|^2 - \alpha_{ee})}{\alpha_{ee}} = -2(2 + q)\alpha_{ee} \\ &= -\frac{(2 + q)Y^2}{1 + Y^2 + (q/2)Y^2}, \end{aligned} \quad (38b)$$

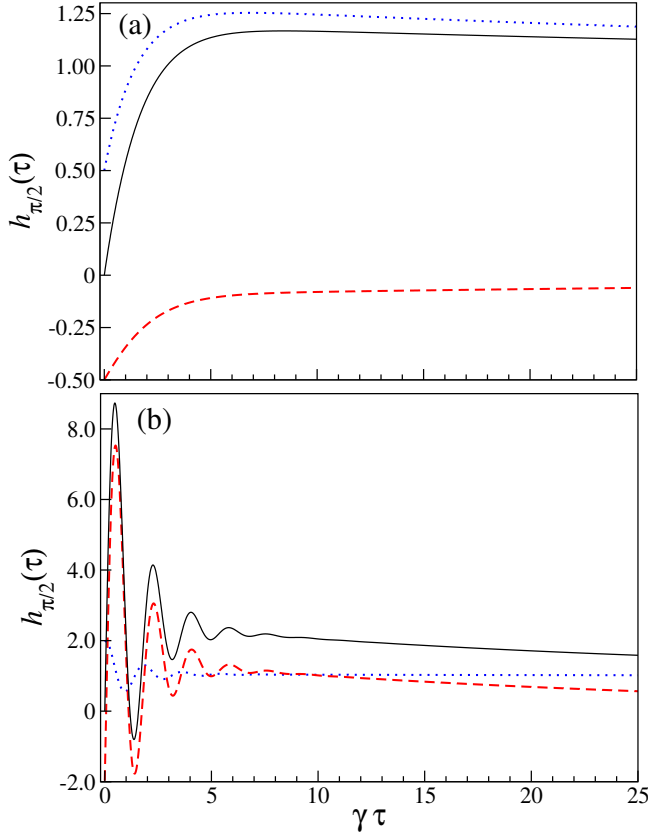


FIG. 6: (Color online) Amplitude-intensity correlation $h_{\pi/2}(\tau)$ (solid black line) and its parts $1 + h_{\pi/2}^{(2)}(\tau)$ (dotted blue line) and $h_{\pi/2}^{(3)}(\tau)$ (dashed red line) for (a) $\Omega = \gamma_+/4 = 0.2625\gamma$ and (b) $\Omega = 3.5\gamma$. The other parameters are $\gamma_d = 0.05\gamma$ and $\gamma_a = 0.015\gamma$. Only the analytical results are plotted.

that is, the initial size of the correlation is proportional to the mean population in the excited state. For $\Omega \gg \gamma$, the third-order correlation has its largest (negative) initial value $h_{\pi/2}^{(3)}(0) \rightarrow -2$.

The third-order term signals the deviation from Gaussian fluctuations as a consequence of the nonlinearity of the resonance fluorescence process for increasing laser intensity [22, 23]. As perhaps best noticed in the spectral domain, it is the enhanced sensitivity to nonlinearity that makes CHD stand out over BHD and the spectrum of squeezing. We illustrate this in the next section.

VI. QUADRATURE SPECTRA FROM CHD

The spectrum measured from the amplitude-intensity correlation is given by

$$\mathcal{S}_\phi(\omega) = 4\gamma_+\alpha_{ee} \int_0^\infty d\tau \cos \omega\tau [h_\phi(\tau) - 1]. \quad (39)$$

The factor $4\gamma_+\alpha_{ee}$ is the photon flux into the CHD setup. For $\phi = 0$ we replace it by $4\gamma_+(\alpha_{ee} + E_{\text{off}}^2)$. Following

the splitting of $h_\phi(\tau)$, Eq. (36a), the spectra of second- and third-order dipole fluctuations are, respectively,

$$\mathcal{S}_\phi^{(2)}(\omega) = 4\gamma_+\alpha_{ee} \int_0^\infty d\tau \cos \omega\tau h_\phi^{(2)}(\tau), \quad (40a)$$

$$\mathcal{S}_\phi^{(3)}(\omega) = 4\gamma_+\alpha_{ee} \int_0^\infty d\tau \cos \omega\tau h_\phi^{(3)}(\tau), \quad (40b)$$

Using Eqs. (33) and (34) we obtain the approximate analytical spectra. For $\phi = 0$, we have

$$\mathcal{S}_0(\omega) = -4\gamma_+\alpha_{ee} \frac{\lambda_1}{\omega^2 + \lambda_1^2}, \quad (41)$$

which is independent of the offset. The spectrum of this quadrature is a simple Lorentzian of width $\gamma_+/2$. For $\phi = \pi/2$ we have

$$\mathcal{S}_{\pi/2}(\omega) = 4\gamma_+\alpha_{ee} \left[B_+ \frac{\lambda_+}{\omega^2 + \lambda_+^2} + B_- \frac{\lambda_-}{\omega^2 + \lambda_-^2} - B_2 \frac{\lambda_2}{\omega^2 + \lambda_2^2} \right]. \quad (42)$$

The second-order spectra are

$$\mathcal{S}_0^{(2)}(\omega) = \mathcal{S}_0(\omega), \quad (43a)$$

$$\mathcal{S}_{\pi/2}^{(2)}(\omega) = 8\gamma_+ \left[C_+ \frac{\lambda_+}{\omega^2 + \lambda_+^2} + C_- \frac{\lambda_-}{\omega^2 + \lambda_-^2} - C_2 \frac{\lambda_2}{\omega^2 + \lambda_2^2} \right]. \quad (43b)$$

These are just the spectra of squeezing, Eqs. (26) and (27), without the detector efficiency factor. The third-order spectra are

$$\mathcal{S}_\phi^{(3)}(\omega) = \mathcal{S}_\phi(\omega) - \mathcal{S}_\phi^{(2)}(\omega) \quad (44a)$$

$$\mathcal{S}_0^{(3)}(\omega) = 0, \quad (44b)$$

$$\mathcal{S}_{\pi/2}^{(3)}(\omega) = -4\gamma_+\alpha_{ee} \sum_{k=2,+,-} D_k \frac{\lambda_k}{\omega^2 + \lambda_k^2}, \quad (44c)$$

where D_k are given by Eq. (37c) and λ_k are the eigenvalues Eq. (10).

Originally, CHD was conceived to overcome the issue of imperfect detection and thus be able to measure squeezing of weak light sources [13, 14]. In the weak-field limit the spectrum of the amplitude-intensity correlation approaches the spectrum of squeezing if third-order fluctuations can be neglected, i.e.,

$$\mathcal{S}_\phi(\omega) = \eta \mathcal{S}_\phi^{(2)}(\omega) \approx \eta \mathcal{S}_\phi(\omega). \quad (45)$$

For the third-order spectrum, the sharp peak is about half the second-order one, of size $\sim Y^4$, while the other terms go also as Y^4 , and the other second-order terms go as Y^2 . However, for not-so-weak fields, we find strong signatures of third-order fluctuations in the spectra.

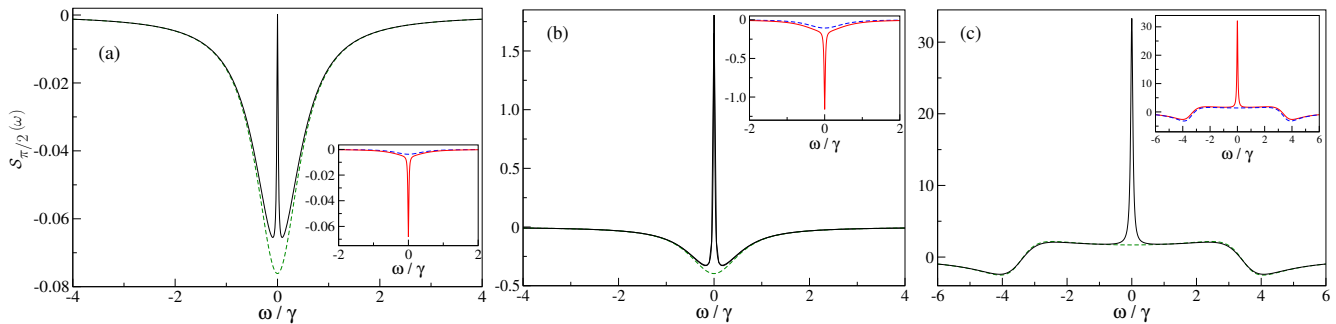


FIG. 7: (Color online) Spectra of the amplitude-intensity correlation for $\phi = \pi/2$ of the three-level atom (solid black line) and two-level atom (dashed green line): (a) weak field $\Omega = 0.1\gamma$, (b) moderate field $\Omega = \gamma_+/4 = 0.2625\gamma$, and (c) strong field $\Omega = 3.5\gamma$. The insets show the third-order spectra of the 3LA (solid red line) and 2LA (dashed blue line). The second-order spectra are those of the spectrum of squeezing (Fig. 3). Only the analytical results are plotted.

In Fig. 7 we plot the analytical results of the spectra of the amplitude-intensity correlation of the two- and three-level atom, Eq. (42). The difference from the (omitted) exact results is very small. Note that for weak and saturating laser the sharp peak is smaller than in the spectra of squeezing, Fig. (3). This is because the third-order

sharp peak is negative in this excitation regime, as seen in the insets. Moreover, in this excitation regime, the full third-order spectrum is negative [insets of Figs. 7(b) and 7(c)], which adds to the negative squeezing peak of this quadrature [22, 23].

In the strong-excitation regime the third-order spectrum leads to striking deviations between the CHD and squeezing spectra and between the 2LA and the 3LA. On the one hand, the sidebands become dispersive [22]. This comes out when λ_{\pm} become complex, that is, for $\Omega > \gamma_+/4$, but it is only for strong enough excitation that the spectral components split. While the second-order peaks are Lorentzians, the third-order ones are dispersive and of comparable size for the 2LA [22] or bigger for the 3LA. On the other hand, there are large deviations in the size of the spectra. The third-order spectrum is much bigger in the 3LA than in the 2LA, not only for the sharp peak. The third-order spectrum contributes most of the total CHD spectrum.

The above effects can be explained as follows. The third-order correlation of fluctuation operators gives a measure of the atom-laser nonlinearity, which grows with increasing laser intensity, and the deviation from Gaussian fluctuations of the fluorescence. Also, it should be mentioned that the dipole fluctuations of the driven transition are enhanced due to the coupling to the long-lived state $|a\rangle$, which is populated by the increased number of spontaneous emission events from the excited state, Eq. (6d). An early study of this effect in the three-level configuration of this paper reported large deviations in the photon statistics from those of a 2LA [33].

We recall that in CHD the second- and third-order

components cannot be measured separately; both are merged in a single measured signal. CHD goes beyond the concept of squeezing when studying phase-dependent fluctuations.

A. Integrated spectra

Finally, we calculate the integrated spectra of the CHD quadratures:

$$\int_{-\infty}^{\infty} S_0(\omega) d\omega = 4\pi\gamma_+\alpha_{ee}, \quad (46a)$$

$$\int_{-\infty}^{\infty} S_{\pi/2}(\omega) d\omega = -4\pi\gamma_+\alpha_{ee}. \quad (46b)$$

That the magnitudes are equal means that the total emitted noise is independent of the quadrature. This is made possible by the third-order fluctuations, absent in the spectrum of squeezing, Sec. IV A. This result is analogous to calculating the total incoherent emission by integrating the incoherent spectrum.

VII. CONCLUSIONS

We investigated ensemble-averaged phase-dependent fluctuations of the intermittent resonance fluorescence of

a single three-level atom. We focused mainly on the spectrum of squeezing by balanced homodyne detection, and on the spectrum of the amplitude-intensity correlation of conditional homodyne detection. The shelving effect produces a sharp peak in the spectrum of the quadrature that features squeezing. Since this peak is positive, it acts to reduce the amount of squeezing observed in the weak- to moderate- (strong-) excitation regime. Since CHD is sensitive to third-order dipole fluctuations that grow with atom-laser nonlinearity, the spectra of BHD and CHD are very different for strong excitation. Additional insight is obtained by calculating the variances or integrated spectra of quadratures. In BHD the variances are different, while in CHD they are equal, a feature that deserves further study.

We considered only the case of exact atom-laser resonance. This allowed us to obtain a very good approximate analytical solution of the master equation with a simple method, which we then used to construct analytical expressions for the various quantities of interest. Further insight into the incoherent spectrum and its link

to the phase-dependent fluctuations could be established. Also, the on-resonance case allowed us to present the basic physical features in the most straightforward manner.

Conditional homodyne detection, with its sensitivity to third-order field fluctuations, opens a new gate to study phase-dependent fluctuations beyond the realm of squeezing for highly nonlinear and non-Gaussian optical processes. On the other hand, the impressive advances in photon collection efficiencies by parabolic mirrors [10, 34] could complement CHD for atomic resonance fluorescence, its squeezing and its quantum fluctuations in general.

Acknowledgments

H.M.C.-B thanks Prof. J. Récamier for hospitality at ICF-UNAM. R.R.A thanks CONACYT for the scholarship No. 379732, and DGAPA-UNAM for support under project IN108413.

Appendix A: Approximate Solutions

The approximate expectation values of the atomic operators are

$$\langle \sigma_{\mp}(t) \rangle = \mp i \frac{Y/\sqrt{2}}{1+Y^2} \left[e^{\lambda_2 t} - e^{-3\gamma_+/4} \left(\cosh \delta t + \frac{3\gamma_+}{4\delta} \sinh \delta t \right) \right] \mp i\sqrt{2}Y \frac{\gamma_+}{4\delta} e^{-3\gamma_+/4} \sinh \delta t + \alpha_{\mp} (1 - e^{\lambda_2 t}) , \quad (\text{A1a})$$

$$\langle \sigma_{ee}(t) \rangle = \frac{Y^2/2}{1+Y^2} \left[e^{\lambda_2 t} - e^{-3\gamma_+/4} \left(\cosh \delta t + \frac{3\gamma_+}{4\delta} \sinh \delta t \right) \right] + \frac{Y^2/2}{1+Y^2 + (q/2)Y^2} (1 - e^{\lambda_2 t}) , \quad (\text{A1b})$$

$$\langle \sigma_{gg}(t) \rangle = e^{\lambda_2 t} - \frac{Y^2/2}{1+Y^2} \left[e^{\lambda_2 t} - e^{-3\gamma_+/4} \left(\cosh \delta t + \frac{3\gamma_+}{4\delta} \sinh \delta t \right) \right] + \frac{1 + (Y^2/2)}{1+Y^2 + (q/2)Y^2} (1 - e^{\lambda_2 t}) . \quad (\text{A1c})$$

We make several assumptions to give our results simple, albeit long, expressions: First, we neglect a term $\gamma_d \Omega^2/2$ in the solutions in the Laplace space that reduce the problem to one similar to the 2LA case, with γ replaced by γ_+ . Eigenvalues λ_{\pm} are thus identified. They give rise to the terms with the hyperbolic functions. Second, a constant term is multiplied by a factor $e^{\lambda_2 t}$. Finally, we add a term $\langle \sigma_{jk} \rangle_{st} (1 - e^{\lambda_2 t})$. Recall that for the case of a 2LA $\lambda_2 = 0$ and $\langle \sigma_{ee}(t) \rangle + \langle \sigma_{gg}(t) \rangle = 1$. These *ad hoc* assumptions make the approximate solutions very close to the exact ones, as long as γ_d and γ_a are at least one order smaller than γ .

Similarly, we obtain

$$\begin{aligned} \langle \sigma_+(0) \sigma_{\mp}(\tau) \rangle_{st} &= \pm \frac{1}{2} \frac{Y^2}{(1+Y^2 + (q/2)Y^2)^2} + \frac{1}{4} \frac{Y^2}{1+Y^2 + (q/2)Y^2} e^{\lambda_1 \tau} \pm \frac{q}{4} \frac{Y^4}{(1+Y^2)(1+Y^2 + (q/2)Y^2)^2} e^{\lambda_2 \tau} \\ &\mp \frac{1}{4} \frac{Y^2}{(1+Y^2)(1+Y^2 + (q/2)Y^2)} e^{-3\gamma_+/4} \left[(1-Y^2) \cosh \delta \tau \mp \frac{1-5Y^2}{4\delta/\gamma_+} \sinh \delta \tau \right] . \end{aligned} \quad (\text{A2})$$

Appendix B: Equations of motion

We solve sets of linear equations of motion for the expectation values of the atomic operators and for two-time correlations. The equations and the formal solutions can be written as

$$\frac{d}{dt} g(t) = \mathbf{M} g(t) , \quad (\text{B1})$$

$$g(t) = e^{\mathbf{M}t} g(0) , \quad (\text{B2})$$

where \mathbf{M} is the matrix (4b). In general, we solve these equations numerically. The initial conditions, however, are obtained exactly analytically, even off resonance. For instance, defining $\Delta \mathbf{s} \equiv (\Delta \sigma_-, \Delta \sigma_+, \Delta \sigma_{ee}, \Delta \sigma_{gg})^T$, where $\Delta \sigma_{jk} = \sigma_{jk} - \alpha_{jk}$ and $\alpha_{jk} = \rho_{kj}^{st}$, $\alpha_+ = \rho_{ge}^{st}$, $\alpha_- = \rho_{eg}^{st}$, the initial conditions of the second- and third-order correlations of the fluctuation operators are

$$\langle \Delta \sigma_+ \Delta \mathbf{s} \rangle_{st} = \begin{pmatrix} \alpha_{ee} - \alpha_+ \alpha_- \\ -\alpha_+^2 \\ -\alpha_+ \alpha_{ee} \\ \alpha_+ (1 - \alpha_{gg}) \end{pmatrix} = \frac{\Omega^2}{N^2} \begin{pmatrix} (2+q)\Omega^2 \\ \gamma_+^2 \\ -i\gamma_+ \Omega \\ i(1+q)\gamma_+ \Omega \end{pmatrix}, \quad (\text{B3})$$

$$\langle \Delta \sigma_+ \Delta \mathbf{s} \Delta \sigma_- \rangle_{st} = \begin{pmatrix} 2\alpha_- (\alpha_+ \alpha_- - \alpha_{ee}) \\ 2\alpha_+ (\alpha_+ \alpha_- - \alpha_{ee}) \\ \alpha_{ee} (2\alpha_+ \alpha_- - \alpha_{ee}) \\ (\alpha_{gg} - 1) (2\alpha_+ \alpha_- - \alpha_{ee}) \end{pmatrix} = \frac{\Omega^4}{N^3} \begin{pmatrix} i2(2+q)\gamma_+ \Omega \\ -i2(2+q)\gamma_+ \Omega \\ \gamma_+^2 - (2+q)\Omega^2 \\ (1+q)[\gamma_+^2 - (2+q)\Omega^2] \end{pmatrix}, \quad (\text{B4})$$

respectively, where we used the steady-state values α_{jk} of Eqs. (6) and $N = (2+q)\Omega^2 + \gamma_+^2$.

The numerical calculations of the spectra are more efficiently implemented using the formal solution of the correlations, $g(\tau) = e^{\mathbf{M}\tau} g(0)$, so the Fourier integral is formally solved as $(i\omega \mathbf{1} - \mathbf{M})^{-1} g(0)$, where $\mathbf{1}$ is the 4×4 identity matrix. One is saved from potentially troublesome integrals where the upper limit is a long time of the order γ_d^{-1} .

-
- [1] For a review see, e.g., M. B. Plenio and P. L. Knight, *Rev. Mod. Phys.* **70**, 101 (1997).
 - [2] F. D. Stefani, J. P. Hoogenboom, and E. Barkai, *Phys. Today* **62**(2), 34 (2009).
 - [3] G. C. Hegerfeldt and M. B. Plenio, *Phys. Rev. A* **52**, 3333 (1995).
 - [4] B. M. Garraway, M. S. Kim, and P. L. Knight, *Opt. Commun.* **117**, 560 (1995).
 - [5] J. Evers and Ch. H. Keitel, *Phys. Rev. A* **65**, 033813 (2002).
 - [6] V. Büchner and Chr. Tamm, *Phys. Rev. A* **61**, 061801 (2000).
 - [7] J. T. Höffges, H. W. Baldauf, W. Lange, and H. Walther, *J. Mod. Opt.* **44**, 1999 (1997).
 - [8] D. F. Walls and P. Zoller, *Phys. Rev. Lett.* **47**, 709 (1981).
 - [9] M. J. Collett, D. F. Walls, P. Zoller, *Opt. Commun.* **52**, 145 (1984).
 - [10] M. Sonderman and G. Leuchs, in *Engineering the Atom-Photon Interaction*, edited by A. Predojevic and M. W. Mitchell (Springer, Heidelberg, 2015).
 - [11] W. Vogel, *Phys. Rev. Lett.* **67**, 2450 (1991).
 - [12] W. Vogel, *Phys. Rev. A* **51**, 4160 (1995).
 - [13] H. J. Carmichael, H. M. Castro-Beltran, G. T. Foster, and L. A. Orozco, *Phys. Rev. Lett.* **85**, 1855 (2000).
 - [14] G. T. Foster, L. A. Orozco, H. M. Castro-Beltran, and H. J. Carmichael, *Phys. Rev. Lett.* **85**, 3149 (2000).
 - [15] H.-G. Hong, W. Seo, M. Lee, W. Choi, J.-H. Lee, and K. An, *Opt. Lett.* **31**, 3182 (2006).
 - [16] N. B. Grosse, Th. Symul, M. Stobińska, T. C. Ralph, and P. K. Lam, *Phys. Rev. Lett.* **98**, 153603 (2007).
 - [17] L. A. Krivitsky, U. L. Andersen, R. Dong, A. Huck, C. Wittmann, and G. Leuchs, *Phys. Rev. A* **79**, 033828 (2009).
 - [18] B. Kühn and W. Vogel, *Phys. Rev. Lett.* **116**, 163603 (2016); arXiv:1511.01723.
 - [19] H. J. Carmichael, *Phys. Rev. Lett.* **55**, 2790 (1985).
 - [20] C. H. H. Schulte, J. Hansom, A. E. Jones, C. Matthiesen, C. Le Gall, and M. Atatüre, *Nature (London)* **525**, 222 (2015).
 - [21] S. Gerber, D. Rotter, L. Slodička, J. Eschner, H. J. Carmichael, and R. Blatt, *Phys. Rev. Lett.* **102**, 183601 (2009).
 - [22] H. M. Castro-Beltran, *Opt. Commun.* **283**, 4680 (2010).
 - [23] H. M. Castro-Beltran, L. Gutierrez, and L. Horvath, *Appl. Math. Inf. Sci.* **9**, 2849 (2015).
 - [24] A. Denisov, H. M. Castro-Beltran, and H. J. Carmichael, *Phys. Rev. Lett.* **88**, 243601 (2002).
 - [25] E. R. Marquina-Cruz and H. M. Castro-Beltran, *Laser Phys.* **18**, 157 (2008).
 - [26] H. M. Castro-Beltran, L. Gutierrez, and E. R. Marquina-Cruz, in *Latin America Optics and Photonics*, Cancun, Mexico, 2014, OSA Technical Digest (Optical Society of America, Washington, D.C., 2014), paper LM4A.38.
 - [27] Q. Xu, E. Greplova, B. Julsgaard, and K. Mølmer, *Phys. Scripta* **90**, 128004 (2015).
 - [28] Q. Xu and K. Mølmer, *Phys. Rev. A* **92**, 033830 (2015).
 - [29] H. J. Carmichael, *Statistical Methods in Quantum Optics 1: Master Equations and Fokker-Planck Equations* (Springer, Berlin, 2002).
 - [30] B. R. Mollow, *Phys. Rev.* **188**, 1969 (1969).
 - [31] P. R. Rice and H. J. Carmichael, *J. Opt. Soc. Am. B*, **5**, 1661 (1988).
 - [32] H. J. Carmichael, *J. Opt. Soc. Am. B*, **4**, 1588 (1987). The ideal source field spectrum of squeezing is the one produced by the (atomic) source alone, neglecting the free field. Since the latter is assumed to be in the vacuum state, its omission is justified on the basis of using normal and time operator orderings.
 - [33] M. Merz and A. Schenzle, *Appl. Phys. B* **50**, 115 (1990).
 - [34] M. Stobińska, M. Sonderman, and G. Leuchs, *Opt. Commun.* **283**, 737 (2010).